Iranian Journal of Materials Forming

Research Article

Locally Lateral Upsetting of Metal Rods: Theoretical Analysis and Experimental Verification

P. Fahimi and H. Haghighat*

Mechanical Engineering Department, Razi University, Kermanshah, Iran

ARTICLE INFO

ABSTRACT

This paper investigates the locally lateral upsetting process of the metal through an analytical and experimental approach. A mathematical model is proposed to calculate the variation in the width of the contact area between the rod and the cylindrical-shaped dies. Additionally, the upsetting load curve is estimated using the slab analysis method. To validate the analytical model, multiple experiments were conducted using aluminum and copper rods. The process was further simulated using DEFORM 3D software. Finally, the influence of key parameters, including the initial rod diameter, rod material, and die diameter on the contact width and upsetting load was analyzed, and compared across different methods. The results show a strong correlation between analytical, experimental, and finite element (FE) data, demonstrating the proposed analytical method is an efficient tool for designing and optimizing the locally lateral upsetting process, reducing both time and cost.

1. Introduction

Due to the difficulty of forming complex shapes in a single step, multi-step forming is often necessary. One common approach in manufacturing automotive components such as connecting rods, tie rods, and crankshafts is the local lateral upsetting of metal rods. In this process, a rod is placed horizontally between two dies, which then move toward each other. The application of compressive force induces plastic deformation, shaping the material accordingly. As with other metal forming techniques, optimizing the local lateral upsetting process is crucial for industrial applications and manufacturers. A well-engineered design, including the careful selection of process parameters, ensures an efficient and cost-effective production process while achieving the desired final

* Corresponding author
  E-mail address: hhaghighat@razi.ac.ir (H. Haghighat)
https://doi.org/10.22099/IJMF.2025.51979.1312

product. Additionally, accurately estimating the required external load and predicting the dimensions of the deformed zone are key factors in enhancing process efficiency and reliability.

In recent years, numerous researchers have analyzed and explored the upsetting process and its various applications. For instance, Vilotic and Shabaik [1] investigated the symmetrical upsetting of sheets using cylindrical-shaped dies through the slab method, conducting a series of experiments. Their study focused on the effects of the die radius and the friction coefficient on the stress distribution within the deformation zone. Lin [2] investigated the upsetting of sheets with concave curved dies as a plane strain process, modeling the die curve as a second-order polynomial function. The theoretical predictions were then with finite element (FE) simulation results obtained using DEFORM 2D software. Essa et al. [3] analyzed the behavior of bi-metallic rod components during the axial upsetting process using both FE simulation and experiment validation. Their primary objective was to assess how the contact between the core and the shell was maintained throughout the process. Similarly, Khanawapee and Butdee [4] investigated the shape and radius of the barrel for bi-material rods after the upsetting process. They also calculated the force required for the process using FE simulation with DEFORM software and validated their findings through experimental results.

Several studies have utilized the compression test to estimate the friction coefficient or friction factor between two materials. For instance, Khoddam et al. [5] proposed a method to determine the friction factor based on the initial and deformed dimensions of the sample.

Hetz et al. [6] developed an approach using the upsetting test with miniaturized cylindrical specimens to investigate the mechanical properties of sheet metal parts with complicated geometries and limited sizes, where extracting conventional specimens for standardized tests is challenging. Their study also analyzed the strain-hardening behavior of the material. Similarly, Ji et al. [7] conducted the cylinder compression test to examine and compare different

materials across a wide temperature range, focusing on material flow characteristics and macroscopic formability.

Fan et al. [8] introduced a novel method called cone end billet upsetting (CEBU), which involves shaping the billet end into a conical form before processing to reduce friction between the billet and the anvil. This approach aimed to prevent the bulging in billets with a high height-to-diameter ratio, a common issue in the traditional upsetting process.

Flattened wire or rod is widely used in various applications, such as manufacturing saw blades, piston rings, and spring wires [9]. In recent years, most studies on flattened rod production have focused on the rolling process. Among these, Kazeminezhad and Karimi Taheri [10] examined the effects of height reduction, rolling speed, and wire material on the contact width between the wire and rolls, as well as the lateral deformation in the wire flat rolling process. They found that the contact width is significantly influenced by height reduction and the wire's initial diameter, proposing a formula to calculate contact width between the wire and rolls. In a subsequent study, Kazeminezhad and Karimi Taheri [11] experimentally evaluated the impact of various parameters on rolling force and wire deformation behavior in the symmetrical rolling process. Continuing their research, they [12] applied the slab method to analyze the symmetrical wire rolling process, predicting rolling pressure distribution and the required rolling force. They derived governing equations by considering changes in the contact width between the wire and rolls as a function of the wire's instantaneous height in the deformation zone. Moreover, Kazeminezhad et al. [13] compared the final cross-sectional profile in the wire flat rolling process using experimental, analytical, and numerical methods across different levels of height reduction. They aimed to compare the accuracy and capability of these methods and to choose the best method based on simplicity and accuracy based on each specific process condition. The entire rod surface is uniformly deformed in flattened rods produced using processes such as rolling. However, in some applications, locally flattened rods are required.

One of the few studies conducted in this field was by Nomura et al. [14], who investigated the asymmetric deformation behavior of rods in a locally lateral upsetting process. They used a flat, fixed lower die and a movable cylindrical upper die with a nose. The effects of different angles of the upper die relative to the rod's axial direction and the nose radius of the upper die on rod deformation and material flow were experimentally analyzed.

Bina and Haghighat [15] studied the lateral compression process of rods between flat dies. They considered plane strain conditions, and the main goal of their work was to predict the cross-sectional deformed shape of the rod and estimate the force required for the process.

According to the aforementioned points, the locally lateral upsetting process of the rod has not been thoroughly analyzed. Implementing this process provides a suitable method to quickly and simply predict the effect of various parameters, such as height reduction, rod material, die radius, and friction coefficient, on the process.

Most studies on the upsetting process focus on situations where rods undergo axial compression loading or where their entire length is subjected to lateral compression loading. This paper investigates the plastic deformation of a rod segment under lateral compression loading. A relationship is proposed to determine the width of the contact area between the rod and the dies, considering the effects of key parameters. Next, the locally lateral upsetting process is analyzed using the slab method, and the force required for the upsetting process under different conditions is calculated. Furthermore, experiments and DEFORM 3D simulations are conducted to evaluate the accuracy of the analytical method and assess the effect of varying parameters on the process. Ultimately, a strong consistency is observed between analytical, simulation, and experimental results.

2. Theoretical Analysis

2.1. Geometric relations

Fig. 1(a) shows the schematic illustration of the locally

lateral upsetting process of a rod using cylindrical dies. The metal rod is placed horizontally between two identical cylindrical dies-upper and lower. As shown in Fig. 1(a), the rod's axis is perpendicular to the dies' longitudinal axis. The lower die is fixed, while the upper die is attached to the ram. By applying a compressive force, the dies move toward each other, causing plastic deformation in a specific section of the rod. The initial rod diameter is denoted as $d_0 (= h_0)$, and the die radius is R. Fig. 1(b) presents the Cartesian coordinate system used for the analysis, with the origin located at the intersection of the rod's axis of symmetry and the mid-plane in the vertical rod. The initial and deformed cross-sections of the rod are shown in Figs. 1(a) and 1(b), respectively. In addition, Fig. 1(b) illustrates the width and height of the deformed cross-sections at $x=0$, b_1, and h_1, and an arbitrary distance from the origin as b and h. Due to the change in rod width within the deformation zone, the locally lateral upsetting process cannot be considered a plane strain one. Therefore, to analyze it, the variation in the width of the contact area between the rod and the dies (i.e., the value of b in Fig. 1(b)) must be determined throughout the upsetting process. To derive the relationship for calculating b, first, the rod's cross-section at the start of the process is considered, as shown in Fig. 2(a).
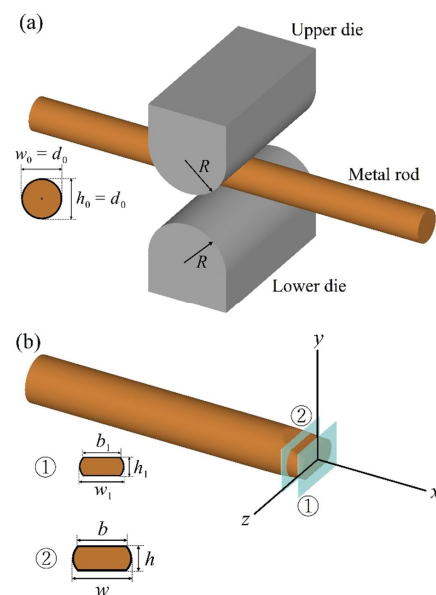

Fig. 1. (a) Schematic illustration of the locally lateral upsetting process of a rod and (b) deformed cross-sections at an arbitrary distance from the origin and at $x=0$.
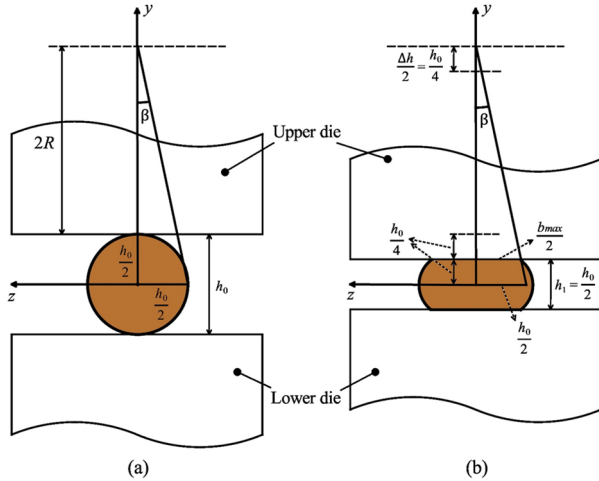
Fig. 2. The width of the contact area in the rod cross-section at *x=0*; (a) before and (b) after the process.

A line is drawn from the point located at a distance of *2R* in the *y* direction to the end of the rod's horizontal diameter. According to Fig. 2(a), the slope of this line is calculated as follows:

$$\tan\beta = \frac{h_0}{4R + h_0} \tag{1}$$

Fig. 2(b) is drawn assuming a maximum reduction of 50%, which is often suitable for the upsetting process. Additionally, assuming that the point corresponding to the maximum reduction lies on the line drawn in Fig. 2(a), the value of tan β in Fig. 2(b) is given by:

$$\tan\beta = \frac{2b_{max}}{8R + h_0} \tag{2}$$

Based on Eqs. (1) and (2), we can write:

$$\frac{b_{max}}{2} = \frac{h_0(8R + h_0)}{4(4R + h_0)} \tag{3}$$

The reduction in rod height at each section, i.e., Δh, is defined as follows:

$$\Delta h = d_0 - h = h_0 - h \tag{4}$$

Where *h* represents the rod height during the process. By considering a second-order polynomial between *b/2* and $\Delta h/2$ (i.e., the variation in rod height during different strokes of the die) and applying the boundary conditions shown in the figure, we obtain:

$$\begin{cases} at\ \frac{b}{2} = 0\ \rightarrow\ \frac{\Delta h}{2} = 0, \dfrac{d\left(\frac{\Delta h}{2}\right)}{d\left(\frac{b}{2}\right)} = 0 \\ at\ \frac{b}{2} = \frac{b_{max}}{2}\ \rightarrow\ \frac{\Delta h}{2} = \frac{h_0}{4} \end{cases} \tag{5}$$

The relationship between *b* and Δh can be expressed as:

$$b = \sqrt{\frac{h_0}{2}\frac{(8R + h_0)}{(4R + h_0)}}\sqrt{\Delta h} \tag{6}$$

Using Eq. (6), the corresponding value of *b* can be calculated for any given Δh. The obtained relationship, which shows that *b* is proportional to the square root of Δh, aligns with the results presented by Pater and Weronski [16] for the width of the contact area in cross wedge rolling. It is also consistent with the findings of Pater [17], or the rotational compression of a rod and the model developed by Kazeminezhad and Karimi Taheri [10] for the wire flat rolling process.

2.2. Slab method of analysis

After deriving the equation to calculate the changes in the width of the contact area within the deformation zone, the process was analyzed using the slab method. For this purpose, the following assumptions were made in this study.

1) The dies are considered rigid bodies with no deformation.

2) The rod is assumed to be a rigid-perfectly plastic material, with no strain-hardening effects.

3) The friction coefficient between the rod and the dies remains constant.

Fig. 3 presents a schematic diagram of the upsetting process and the geometrical parameters used in the analysis. The governing equations are derived by combining force equilibrium in the horizontal and vertical directions, applying boundary conditions, yield criteria, and geometric relations.

By specifying the stresses applied to the vertical slab located at a distance *x* from the coordinate origin in the deformation zone, according to Fig. 4, the force equilibrium in the *x* direction can be expressed as:

$$(\sigma_x + d\sigma_x)(b + db)(h + dh) - \sigma_x bh + 2p \sin\alpha \left(\frac{b+b+db}{2}\right) ds - 2\tau \cos\alpha \left(\frac{b+b+db}{2}\right) ds = 0 \quad (7)$$

Ignoring the multiplication of differential terms and arranging the resulting expression gives:

$$\sigma_x bdh + \sigma_x hdb + bhd\sigma_x + 2pb \tan\alpha dx - 2\tau bdx = 0 \quad (8)$$

By writing the force equilibrium in the y direction, the following equation is obtained:

$$\sigma_y = -p - \tau \tan\alpha \quad (9)$$

$$\sigma_y = -p(1 + \mu \tan\alpha) \quad (10)$$

Since the values of μ and $\tan\alpha$ are usually small, their product can be ignored compared to unity, leading to a simplified expression. Using the Tresca yield criterion and assuming that σ_x and σ_y are the principal maximum and minimum stresses, respectively, we obtain:

$$\sigma_x + p = 2k \quad (11)$$

Thus

$$\sigma_x = 2k - p \quad (12)$$

and

$$d\sigma_x = -dp \quad (13)$$

Additionally, based on the geometry of Fig. 3, the following equations are derived:

$$h = h_1 + 2R - 2\sqrt{R^2 - x^2} \quad (14)$$

$$dh = \frac{2xdx}{\sqrt{R^2 - x^2}} \quad (15)$$

Using Eq. (6), we obtain:

$$db = \frac{-xb}{\sqrt{R^2 - x^2}} \frac{dx}{2\sqrt{R^2 - x^2} - 2R + s} \quad (16)$$

Substituting Eqs. (12)-(16) into Eq. (8) gives:

$$\frac{dp}{dx} = \left(\frac{x}{\left(\sqrt{R^2-x^2}\right)\left(2\sqrt{R^2-x^2}-2R+s\right)} - \frac{2\mu}{h_1+2R-2\sqrt{R^2-x^2}} \right) p + \frac{4kx}{\left(h_1+2R-2\sqrt{R^2-x^2}\right)\left(\sqrt{R^2-x^2}\right)} - \frac{2kx}{\left(\sqrt{R^2-x^2}\right)\left(2\sqrt{R^2-x^2}-2R+s\right)} \quad (17)$$
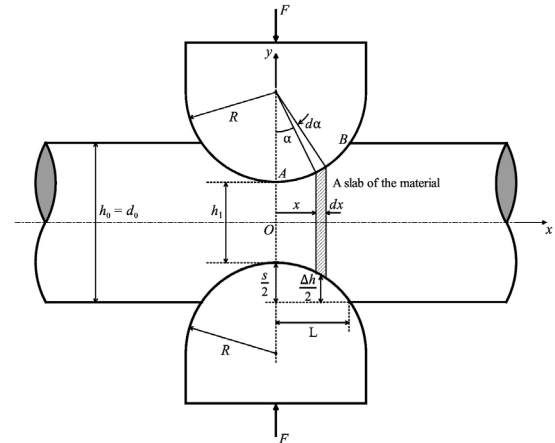

Fig. 3. The configuration of the deformed rod and a slab of the material.
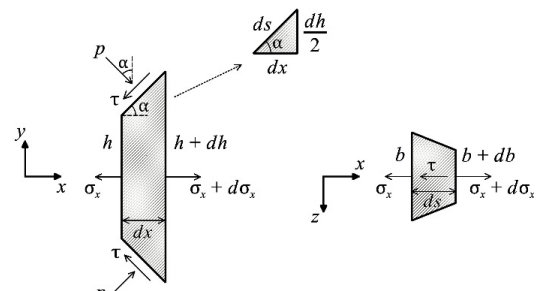

Fig. 4. The stresses acting on the vertical element from different views.

The above differential equation should satisfy the boundary condition that at *x=L*, we have $\sigma_x = 0$, and thus *p=2k*. This equation was solved using a modified Euler numerical method implemented in MATLAB. Moreover, the pressure distribution in the upsetting process was determined. Finally, to compute the required forming load, given the pressure distribution on the contact surface, we use:

$$dF = 2(p\cos\alpha + \tau\sin\alpha)\left(\frac{b+b+db}{2}\right)ds \quad (18)$$

$$F = 2\int_0^L pb\left(1 + \frac{\mu x}{\sqrt{R^2 - x^2}}\right)dx \quad (19)$$

Where *F* is the forming load and *L* is the length of the deformation zone. According to Fig. 3, Eq. (19) can be written as:

$$L = \sqrt{Rs - \frac{s^2}{4}} \quad (20)$$

3. Experiments

Numerous experiments were conducted to verify the accuracy and validity of the theoretical solution proposed in this study, particularly Eq. (6), which was derived to estimate the width of the contact area. All experiments were performed using the SANTAM STM-150 device, as shown in Fig. 5. The tests were carried out using copper and aluminum rods, and the effect of different parameters on the test results was examined. Three different sets of rods were used: copper rods with diameters of 10 mm and 12 mm, and aluminum rods with a diameter of 9.8 mm. Moreover, two sets of dies, made of CK45 steel, were used, with diameters of 20 mm and 30 mm.

Before conducting the upsetting experiments, multiple tensile tests were performed on the materials following the ASTM E8M standard. The tests were carried out to determine the mechanical properties of the materials. The true stress-true strain curves obtained from the tensile tests for both materials are presented in Fig. 6. Additionally, the stress-strain relationships for copper and aluminum used in this study are approximated using the Hollomon equation, as follows:

$$\sigma = 396 \cdot 3 \, \varepsilon^{0 \cdot 0388} \text{ MPa} \tag{21}$$

$$\sigma = 238 \cdot 8 \, \varepsilon^{0 \cdot 1928} \text{ MPa} \tag{22}$$

The specifications of the experiments are provided in Table 1. The die speed was set to 1 mm/min, and all tests were conducted at room temperature without lubrication. To ensure more reliable results, some experiments were repeated under the same conditions. Due to the strains and elastic deformations of the components in the experimental setup, the final height of the sample for a given die stroke, as recorded in the output diagram of the device, may slightly differ from the expected height. This difference depends on the force required for rod deformation.

Finally, after each test, the compression load-stroke diagram generated by the software connected to the device, along with the geometric dimensions of the deformed sample, was recorded as the experiment's output. Fig. 7 presents an example of the output diagram

for case 11 in Table 1. Additionally, Fig. 8 shows the dies and specimens after the upsetting process.
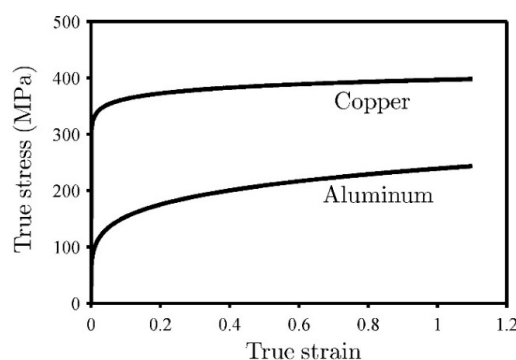

Fig. 5. Experimental setup.

Fig. 6. True stress-true strain curves for aluminum and copper.

Table 1. Process conditions

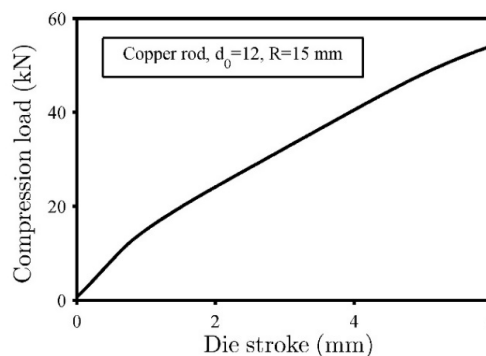| Case	Rod material	Rod diameter (mm)	Die diameter (mm)	*Δh* (mm)
1	Cu	10	30	2.4
2	Cu	10	30	3.3
3	Cu	10	30	4.2
4	Cu	10	20	4.2
5	Al	9.8	30	2.8
6	Al	9.8	30	3.7
7	Al	9.8	30	4.7
8	Al	9.8	20	4.7
9	Cu	12	30	2.9
10	Cu	12	30	4
11	Cu	12	30	5.1
12	Cu	12	20	5.1

Fig. 7. Experimental compression load-stroke diagram for case 11 in Table 1.
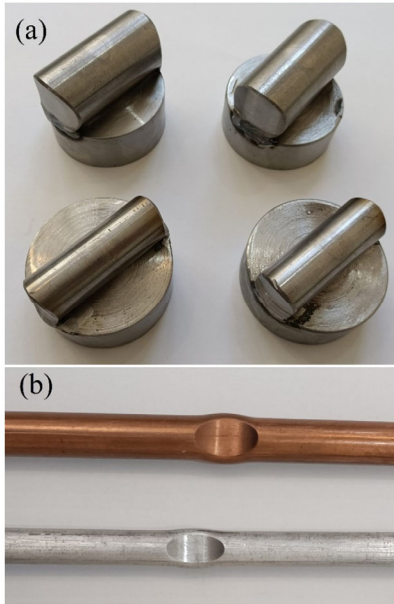
Fig. 8. (a) Two series of made dies, and (b) aluminum and copper samples after deformation (cases 7 and 11 in Table 1).

4. FEM Simulation

In the previous section, several experiments were conducted under different conditions to validate the analytical method. However, due to the limited number of experiments, the expansion of metal forming processes, and the need for efficient use of financial resources and time, there is a growing preference for simulation methods over the trial-and-error approaches when designing tools and dies for forming processes and assessing the effects of various parameters.

The experimental results were used to validate the simulation models. Accordingly, the simulation method can be applied to perform preliminary analyses across a broader range of geometries and process conditions.

In this research, DEFORM 3D software was used to simulate the locally lateral upsetting process of the rod. All cases from the experiments (Table 1) were simulated using the same dimensions and parameters. The dies were modeled as rigid bodies, moving toward each other at a constant velocity in the vertical direction. For each simulation case, the stress-strain behavior of the material was considered in two ways: as a rigid-perfectly plastic material and with strain hardening effects, using Eqs. (21) and (22). The Coulomb friction coefficient (μ) was used to define interface friction between the rod and the dies, as in the analytical analysis developed in section

2.2.

The exact friction coefficient could not be directly measured for input into the theoretical analysis and FEM software. However, the friction coefficient was experimentally determined as 0.11 between copper and steel and 0.02 between aluminum and steel. These values were obtained by measuring the relative change in sample dimensions through experimental methods and comparing them with calibration curves generated from the simulation using friction coefficients ranging from 0.01 to 0.5. The curves plotted to determine the friction coefficient between copper and steel, based on the experiment results of cases 1, 2, and 3 in Table 1, are presented in Fig. 9. As the test results show, the friction coefficient falls within the range of 0.1 and 0.15 (Fig. 9(a)). Additionally, further simulations were conducted to determine the friction coefficient with greater accuracy (Fig. 9(b)).

Figs. 10(a) and 10(b) illustrate the rod's initial and deformed mesh in case 11, which was meshed with 205298 elements, respectively.
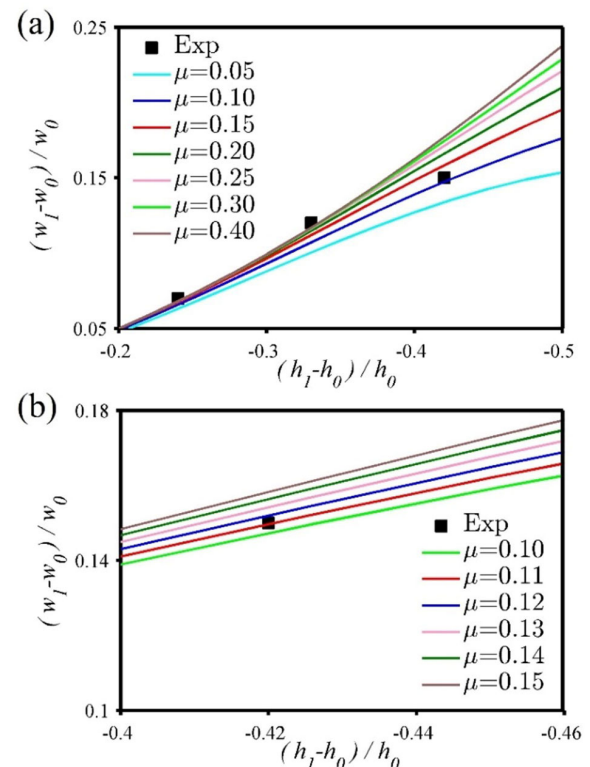

Fig. 9. Dimensionless graphs of simulation results for various friction coefficients with experimentally measured data for the copper rod (d_0=10 mm).
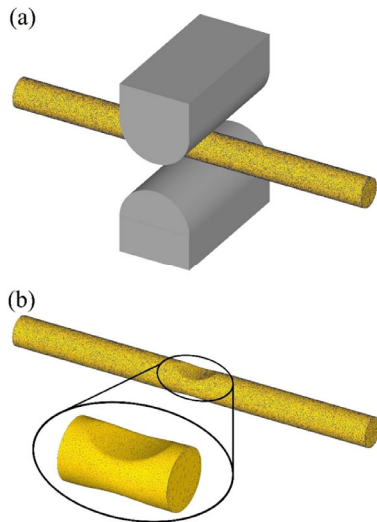
(a)

(b)

Fig. 10. (a) Initial mesh and (b) deformed mesh.

5. Results and Discussion

To confirm the accuracy of Eq. (6), which was derived to calculate the width of the contact area between the rod and the dies, Fig. 11 compares the calculated and experimental values of *b* at different die strokes.

According to the test results, *b* depends on the rod's height reduction. Also, comparing the results for two different initial diameters of copper rods demonstrates the dependence of *b* on the initial diameter of the rod. This dependence is also considered in Eq. (6). According to Fig. 11, the average difference between the results of the theoretical relation in nine measured states and the test results is about 3.7% with a maximum difference of 8.8%.

The effect of changing the radius of the dies on the width of the contact area is represented in Fig. 12. According to the experimental results, *b* varies with changes in the radius of the die. This dependence is also considered in Eq. (6).

The small differences between the test results in Figs. 11 and 12 validate the use of the presented relationship for the width of the contact area in the analysis of the locally lateral upsetting process of the rod.

In the analysis of the process using the slab method in section 2.2, it was assumed that the rod material is rigid-perfectly plastic. In this section, the results of this assumption are compared with those obtained by considering the actual behavior of the material with

strain-hardening effects for the various cases in Table 1. To this end, simulations were performed for both material behavior models. According to the results (Fig. 13), in most cases, the difference between the forces required for forming in the two models is less than 10%, with a maximum difference of 11.7%. Therefore, based on these results and the simplifications made during the theoretical analysis, the rigid-perfectly plastic assumption is acceptable.
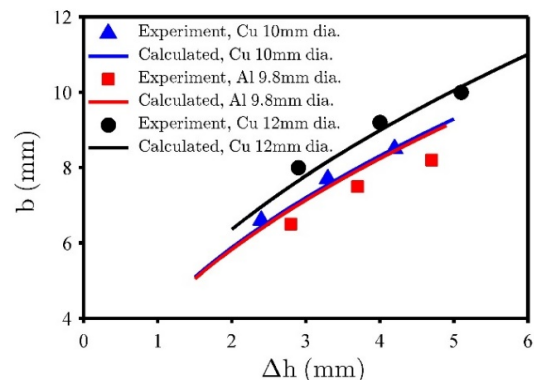

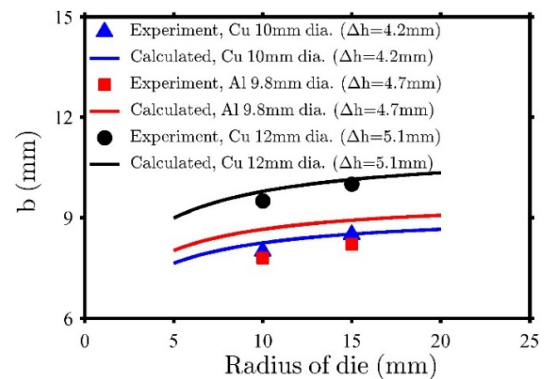**Fig. 11.** The effect of die stroke on the width of the contact area (*R*=15 mm).

Fig. 12. The effect of die radius on the width of the contact area.
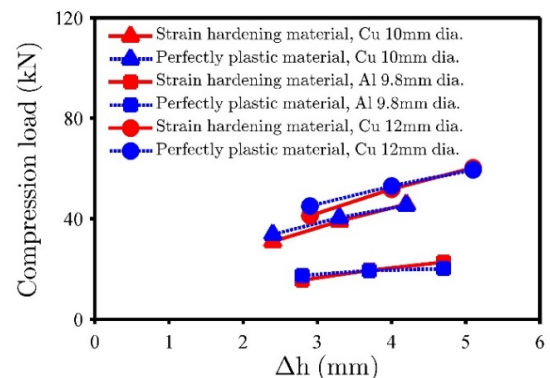

Fig. 13. Simulation results of the compression load for various material behaviors (*R*=15 mm).

The accuracy and correctness of the analytical and simulation results were validated by comparing the compression load at different strokes of the die for a copper rod with an initial diameter of 10 mm, an aluminum rod with a diameter of 9.8 mm, and a copper rod with a diameter of 12 mm with the experimental results in Figs. 14, 15, and 16, respectively. As shown, the load obtained from the simulation aligns more closely with the test results than the load obtained from the slab method. This agreement is expected due to more realistic conditions considered in the simulation.

According to Figs. 14-16, the analytical results are lower than the experimental results. The maximum difference between the analytical and test results is 17.8%. The reasons for this difference stem from the assumptions considered in the process analysis. These assumptions include neglecting the lateral spread (*w* in Fig. 1(b)) when calculating areas in the equilibrium equations and ignoring elastic deformations in the process.
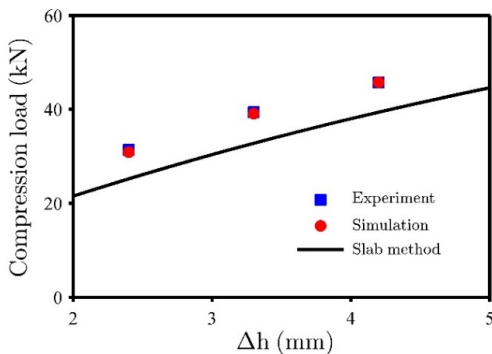

Fig. 16. Comparison of the compression load between experimental results, the theoretical method, and simulation results for a copper rod with a 12 mm diameter (R=15 mm, μ= 0.11).

Moreover, only homogeneous deformations are considered in the slab method. In Fig. 17, to further analyze and compare the data from Figs. 14 and 16, the forming load obtained from different methods for cases 1, 2, 3, 9, 10, and 11 in Table 1 has been plotted.

The difference between the experimental and the simulation results may be due to assumptions such as a constant friction coefficient at the rod-die interface, as well as the approximation of the friction coefficient entered into the software during the simulation process. As the rod's initial diameter increases, the compression load and the contact area between the rod and the dies also increase, leading to higher friction forces at the interface. With increasing strain, and considering the significant impact of friction force on the total deformation force at higher strains, assuming a constant friction coefficient likely contributes to the discrepancy between simulation and experimental results.

Figs. 18, 19, and 20 illustrate the effect of changing the die radius on the compression load at a specific die stroke for a copper rod (10 mm diameter), an aluminum rod (9.8 mm diameter), and a copper rod (12 mm diameter), respectively. As seen in these figures, increasing the die radius leads to a higher force requirement for compression due to the increase in both deformation volume and contact area between the rod and the dies. Both analytical values obtained from the slab method and FEM simulation results align closely with the experimental data, confirming the accuracy of these approaches.

Fig. 14. Comparison of the compression load between experimental results, the theoretical method, and simulation results for a copper rod with a 10 mm diameter (R=15 mm, μ= 0.11).
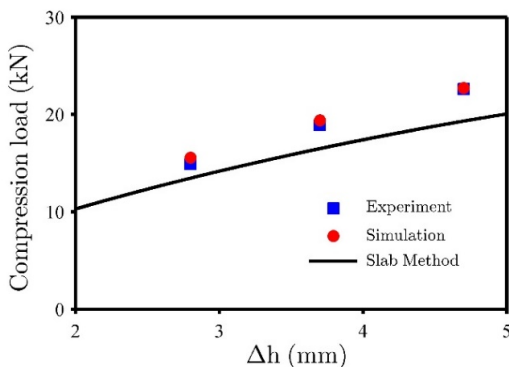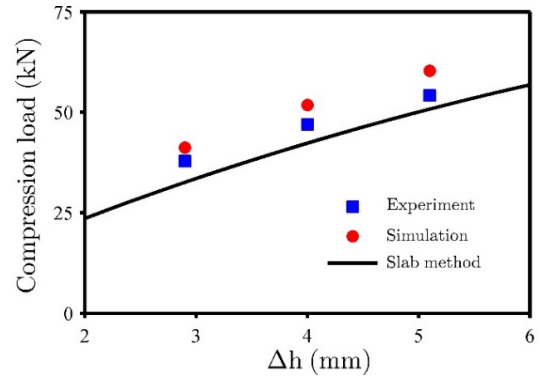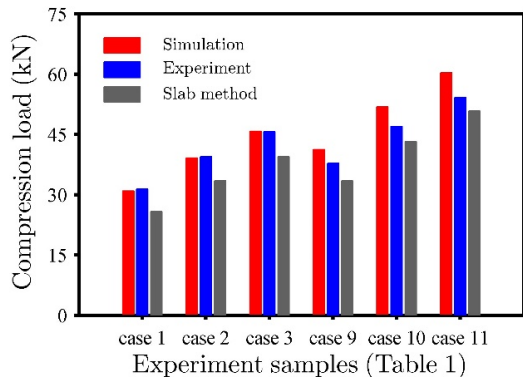

Fig. 15. Comparison of the compression load between experimental results, the theoretical method, and simulation results for an aluminum rod with a 9.8 mm diameter (R=15 mm, μ= 0.02).

Fig. 17. Comparison of simulation and theoretical results with experimental compression load.
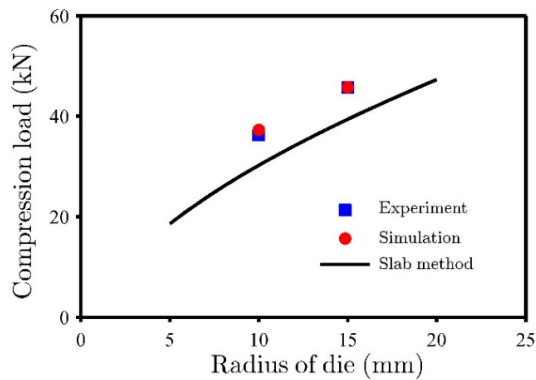

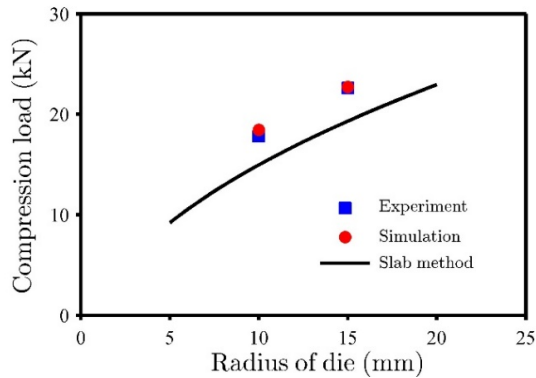**Fig. 18.** Effect of die radius on compression load for a copper rod (10 mm diameter, Δh=4.2 mm, μ= 0.11).

Fig. 19. Effect of die radius on the compression load for an aluminum rod (9.8 mm diameter, Δh=4.7 mm, μ= 0.02).
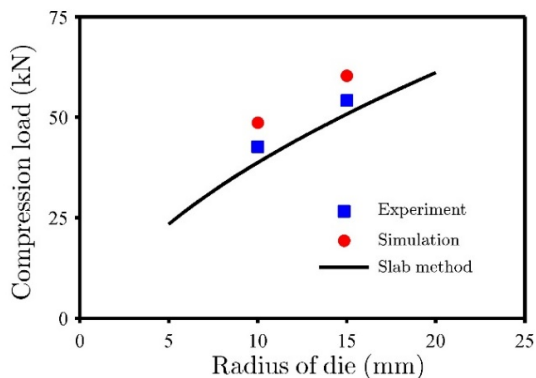

Fig. 20. Effect of die radius on the compression load for a copper rod (12 mm diameter, Δh=5.1 mm, μ= 0.11).

6. Conclusions

This study proposed an analytical model to analyze the locally lateral upsetting process of metal rods using cylindrical-shaped dies. Additionally, an equation was derived to calculate the width of the contact area between the dies and the rod. A comparison between the theoretical predictions and experimental measurements demonstrated the high accuracy of the proposed equation. Moreover, the forming load obtained through the analytical method and FEM simulation was compared with experimental results, revealing that both methods provide reasonable accuracy. However, since the simulation conditions closely resemble the actual process, FEM results exhibited higher accuracy than the analytical approach. Nevertheless, the analytical method remains a valuable tool for predicting and analyzing the process due to its simplicity and high speed in estimating the compression force, along with its ability to evaluate the effects of various conditions and parameters, such as the initial dimensions of rods and dies, height reduction, friction coefficient, and material properties, making it a highly efficient approach. Additionally, it offers a significant reduction in cost and execution time compared to other methods.

Conflict of interest

The authors have no relevant financial or non-financial interests to disclose.

Authors' contributions

All authors contributed equally to the design and execution. All authors have read and approved the final manuscript.

Data availability

All data generated or analyzed in this study are included in this manuscript.

7. References

[1] Vilotic, D., & Shabaik, A. H. (1985). Analysis of upsetting with profiling dies. *Journal of Engineering Materials and Technology, 107*(4), 261-264. https://doi.org/10.1115/1.3225816

[2] Lin, S. Y. (2002). Stress analysis of upsetting with concave curve dies. *Journal of Materials Processing Technology, 123*(1), 36-41. https://doi.org/10.1016/S0924-0136(02)00035-3

[3] Essa, K., Kacmarcik, I., Hartley, P., Plancak, M., & Vilotic, D. (2012). Upsetting of bi-metallic ring billets. *Journal of Materials Processing Technology, 212*(4), 817-824. https://doi.org/10.1016/j.jmatprotec.2011.11.005

[4] Khanawapee, U., & Butdee, S. (2020). A study of barreling and DEFORM 3D simulation in cold upsetting of bi-material. *Materials Today: Proceedings, 26*, 1262-1270. https://doi.org/10.1016/j.matpr.2020.02.252

[5] Khoddam, S., Fardi, M., & Solhjoo, S. (2021). A verified solution of friction factor in compression test based on its sample's shape changes. *International Journal of Mechanical Sciences, 193*, 106175. https://doi.org/10.1016/j.ijmecsci.2020.106175

[6] Hetz, P., Kraus, M., & Merklein, M. (2022). Characterization of sheet metal components by using an upsetting test with miniaturized cylindrical specimen. *CIRP Annals, 71*(1), 233-236. https://doi.org/10.1016/j.cirp.2022.03.010

[7] Ji, S. M., Choi, J. M., & Joun, M. S. (2023). Evaluation of the macroscopic formability of metallic materials using a cylinder compression test. *Journal of Materials Research and Technology, 23*, 2798-2809. https://doi.org/10.1016/j.jmrt.2023.01.173

[8] Fan, J., Liu, Z., Liu, W., & Wang, C. (2023). Simulation and experiment study on cone end billet method in upsetting billet with a large height-to-diameter ratio. *Applied Sciences, 13*(17), 9523. https://doi.org/10.3390/app13179523

[9] Carlsson, B. (1998). The contact pressure distribution in flat rolling of wire. *Journal of Materials Processing Technology, 73*(1), 1-6. https://doi.org/10.1016/S0924-0136(97)00091-5

[10] Kazeminezhad, M., & Karimi Taheri, A. (2005). A theoretical and experimental investigation on wire flat rolling process using deformation pattern. *Materials & Design, 26*(2), 99-103. https://doi.org/10.1016/j.matdes.2004.06.010

[11] Kazeminezhad, M., & Taheri, A. K. (2005). An experimental investigation on the deformation behavior during wire flat rolling process. *Journal of Materials Processing Technology, 160*(3), 313-320. https://doi.org/10.1016/j.jmatprotec.2004.06.020

[12] Kazeminezhad, M., & Karimi Taheri, A. (2006). Calculation of the rolling pressure distribution and force in wire flat rolling process. *Journal of Materials Processing Technology, 171*(2), 253-258. https://doi.org/10.1016/j.jmatprotec.2005.06.070

[13] Kazeminezhad, M., Karimi Taheri, A., & Kiet Tieu, A. (2008). A study on the cross-sectional profile of flat rolled wire. *Journal of Materials Processing Technology, 200*(1), 325-330. https://doi.org/10.1016/j.jmatprotec.2007.09.029

[14] Nomura, T., Nguyen, C. S., Asai, K., & Kitamura, K. (2016). Behavior of asymmetric deformation of rod in locally-lateral upsetting. *Mechanical Engineering Journal, 3*(2), 15-00576. https://doi.org/10.1299/mej.15-00576

[15] Bina, E. P., & Haghighat, H. (2021). Limit analysis of plane strain compression of cylindrical billets between flat dies. *The International Journal of Advanced Manufacturing Technology, 116*(11), 3561-3570. https://doi.org/10.1007/s00170-021-07711-1

[16] Pater, Z., & Weroński, W. (1994). Determination of the contact area between the rolling tools and the workpiece in cross rolling process. *Journal of Materials Processing Technology, 45*(1), 105-110. https://doi.org/10.1016/0924-0136(94)90326-3

[17] Pater, Z. (1996). Analysis of plane-strain rotational compression of rod by FEM. *Journal of Materials Processing Technology, 60*(1), 549-554. https://doi.org/10.1016/0924-0136(96)02385-0